Mon. Not. R. Astron. Soc. **275**, 828–840 (1995)

Low-mass white dwarfs need friends: five new double-degenerate close binary stars

T. R. Marsh,[1] V. S. Dhillon[2] and S. R. Duck[3]

[1] *University of Southampton, Department of Physics, Highfield, Southampton SO17 1BJ*
[2] *Royal Greenwich Observatory, Apartado de Correos 321, Santa Cruz de La Palma, 38780 Tenerife, Canary Islands, Spain*
[3] *University of Oxford, Department of Physics, Nuclear Physics Laboratory, Keble Road, Oxford OX1 3RH*

Accepted 1995 March 2. Received 1995 February 23; in original form 1994 December 2

ABSTRACT

We have discovered five detached close binary stars out of seven white dwarfs chosen for their low mass ($< 0.45\,M_\odot$). The high success rate of our observations supports the notion that evolution within a binary star is needed to obtain white dwarfs with masses below $0.45\,M_\odot$. We have measured the orbital period and radial velocity amplitude of four of our discoveries. No late-type features are seen in any of our targets at a level which forces the mass of any main-sequence companion to be less than $0.1\,M_\odot$. This, together with our measured mass functions, implies that the companion stars are in fact white dwarfs. Our observations raise the number of detached, double-degenerate close binaries with known orbital periods from two to six. All of the orbits are circular, a consequence of past interaction. We find periods of 1.1, 3.3 and 4.8 d for 1713+332, 1241−010 and 1317+453. 2331+290 has a very short period, most likely 4 h, but with the 1 cycle d^{-1} alias at 4.8 h also a possibility. Gravitational radiation will cause this star to merge within about 2×10^9 yr. Close double-degenerates go through one or more stages during which the two stars orbit inside a common envelope. The long orbital periods of 1241−010 and 1317+453 suggest that the ejection of the envelope during the common-envelope phase is very efficient. The spectrum of the companion is directly detectable in 1713+332 but in none of the other systems.

Key words: binaries: close – binaries: spectroscopic – white dwarfs.

1 INTRODUCTION

The possibility that type Ia supernovae might come from merging white dwarfs has provoked considerable interest in finding suitable candidates for such mergers. Several surveys for white dwarf close binary systems have been carried out, without much success. Robinson & Shafter (1987) used a photometric technique to look at 44 white dwarfs, and were sensitive to orbital periods in the range 30 s to 3 h, but they found nothing. Foss, Wade & Green (1991) took spectra of 25 white dwarfs and found no white dwarf binaries, although they did discover radial velocity variation in a subdwarf B star, PG 1538+239; their survey was sensitive to periods from 3 to 10 h. Bragaglia et al. (1990) found one double-degenerate binary star in 54 white dwarfs, plus four other candidate systems.

White dwarf close binary systems are of interest in their own right because they provide constraints upon what is known as the common-envelope phase of evolution (Iben & Livio 1993). This is a stage that has affected or will affect many varieties of binary system. As stars evolve off the main sequence their radius increases, and in a binary orbit this may lead to transfer of mass from one star to its companion. In many cases the companion is unable to accrete the mass at a high enough rate and an envelope forms around both stars. As the stars orbit, angular momentum is transferred from the binary to the envelope which is eventually ejected from the system. Close white dwarf binaries must go through at least one such stage because the second mass transfer stage is from a giant star to a white dwarf, and white dwarfs cannot accrete at high rates.

The ejection of the common envelope can change the parameters of a binary dramatically. For instance the orbital separation may shrink by factor of 1000 or the two stars may even be forced to merge. The efficiency of the ejection is crucial to the eventual outcome. If the envelope ejection is inefficient, requiring large amounts of orbital energy to get rid of the envelope, then the orbit must shrink greatly and short periods or merging will result. On the other hand, merging is less likely if the envelope can be ejected at relatively little cost in terms of orbital energy. The ratio of the envelope binding energy to orbital energy loss, α_{CE}, is therefore of considerable importance in binary star evolution. It is a difficult problem to determine α_{CE} theoretically, and thus an observational calibration is desirable.

Table 1. Instrument configurations.

	WHT/ISIS, 1993		INT/IDS	WHT/ISIS, 1994	
	Blue arm	Red arm		Blue arm	Red arm
FWHM resolution (Å)	0.8	2.8	0.7	1.6	1.8
Wavelength range	6430 – 6760	7700 – 9400	6490 – 6660	4190 – 4990	6130 – 7040
Dispersion (Å/pixel)	0.38	1.4	0.36	0.78	0.74

White dwarf binaries are especially suited to this problem because, once they have emerged from the common envelope, the only significant cause of angular momentum loss is thought to be gravitational radiation. In many cases (for example, the binary stars in this paper), gravitational radiation is too weak to change the period significantly, and we see the binary star essentially as it was once it emerged from its envelope. This contrasts with, for example, cataclysmic variables in which it is thought that other angular momentum loss mechanisms are important.

We started the work for this paper following the work of Bergeron, Saffer & Liebert (1992) who carried out a spectroscopic determination of the masses of 129 DA white dwarfs. They found 14 targets with masses below $0.45\,M_{\odot}$, which is too low for single stars to have achieved within the age of the Galaxy. The obvious alternative is that the evolution of these stars was cut short by mass loss within a binary. In this case, the star can lose its outer envelope without having to reach the asymptotic giant branch or, equivalently, without ever having to ignite helium which requires a core mass of $0.49\,M_{\odot}$ (Sweigart 1994). In order to be seen as a white dwarf, the dimmer component of a white dwarf binary system can only be another compact object or a low-mass main-sequence star, and therefore the last mass transfer event would have been a common-envelope stage. We therefore expect that the low-mass white dwarfs may be members of close binary systems. Our observations were designed to test this prediction. All this assumes that Bergeron et al.'s (1992) analysis produced accurate masses, and therefore our secondary aim was to test this.

2 OBSERVATIONS

The observations were taken over two seasons. In 1993 we used the double-beam spectrograph ISIS on the 4.2-m William Herschel Telescope on La Palma in the Canary Islands to observe seven low-mass white dwarfs. These observations were designed to detect any velocity change and were spread out over the nights of June 11–12, 14–15 and 23–24. All three nights were clear but the second night suffered from very poor seeing (> 2.5 arcsec compared with ≈ 1 arcsec for the other two nights). To make up for this we applied for supplementary observations through the observatory service scheme and obtained spectra of 1614+136 and 1713+332 on June 16–17, and of 2032+188 on August 14–15. We intended originally to observe Hβ and Hγ on the blue arm of ISIS for radial velocities and the TiO band region (7000 to 9000 Å) on the red arm for late-type companions. However, on the advice of R. Saffer we switched to observations of Hα on the blue arm, which forced us to use a dichroic with a cut wavelength of 7500 Å. In doing so we lost the red arm spectrum below 7700 Å but this was compensated by the sharp non-LTE core of Hα possessed by most DA white dwarfs, resulting in improved radial velocity accuracy. Table 1 contains details of the instrument configurations used. In one case, 1241−010, we oriented the slit to place a nearby companion on the slit (Zuckerman & Becklin 1992) in order to separate their spectra as far as possible.

Finally, we obtained more WHT service data on 2331+290 on 1994 July 29–30. In this case we observed Hα on the red arm and Hβ and Hγ on the blue arm.

Our WHT spectra showed obvious radial velocity shifts in some of our targets. Rough estimates suggested that the orbital periods were less than about 10 d, and in order to obtain a long enough run we applied for time on the smaller 2.5-m Isaac Newton Telescope (INT) on La Palma; we were awarded one week. With the INT we could follow three of our detected binaries. We observed with the IDS spectrograph, which has only one camera, and therefore we concentrated on Hα only, our WHT spectra having shown no sign of late-type companions. Again details of the configuration are contained in Table 1. The first night of the INT observations was lost to cloud, and there was partial cloud at the start of the second and through most of the third nights. The fourth, fifth and sixth nights were clear, but dust and poor seeing affected the last night. The dates observed were 1994 April 22–27.

Throughout the observations we were careful to use a narrow slit (0.8 arcsec) to reduce radial velocity errors. Exposure times ranged from 600 to 1800 s according to the brightness of the target, the telescope and the seeing. The spectra were extracted with weights to give the maximum signal-to-noise ratio. Our observing scheme was to take an arc spectrum, one to three object spectra and then another arc spectrum. For each object spectrum the arc spectra were extracted at the same position on the detector and then the wavelength scale derived from the arc pair was interpolated in time for the object spectrum.

The fits to the arc calibrations had rms scatters of about 1/30th of a pixel, and do not significantly increase the uncertainties on our radial velocities which are dominated by photon noise in the spectra.

3 RESULTS

3.1 WHT spectra and the search for late-type companions

We begin the presentation of results with the 1993 WHT run which was designed to detect binary stars. Fig. 1 shows the mean spectra observed during the WHT run. The Hα spectra show the characteristic broad Balmer absorption of white dwarfs, whereas the red spectra are virtually featureless. The red spectra contain no obvious sign of late-type features such as TiO bands which would form an easily recognized pattern. In Fig. 1 we show a spectrum of Gl866A, an M5 dwarf (Kirkpatrick, Henry & McCarthy 1991), for comparison. The contribution from such a late-type spectrum can be estimated by subtracting it from the white dwarf spectrum and then computing the χ^2 between the difference spectrum and a smoothed

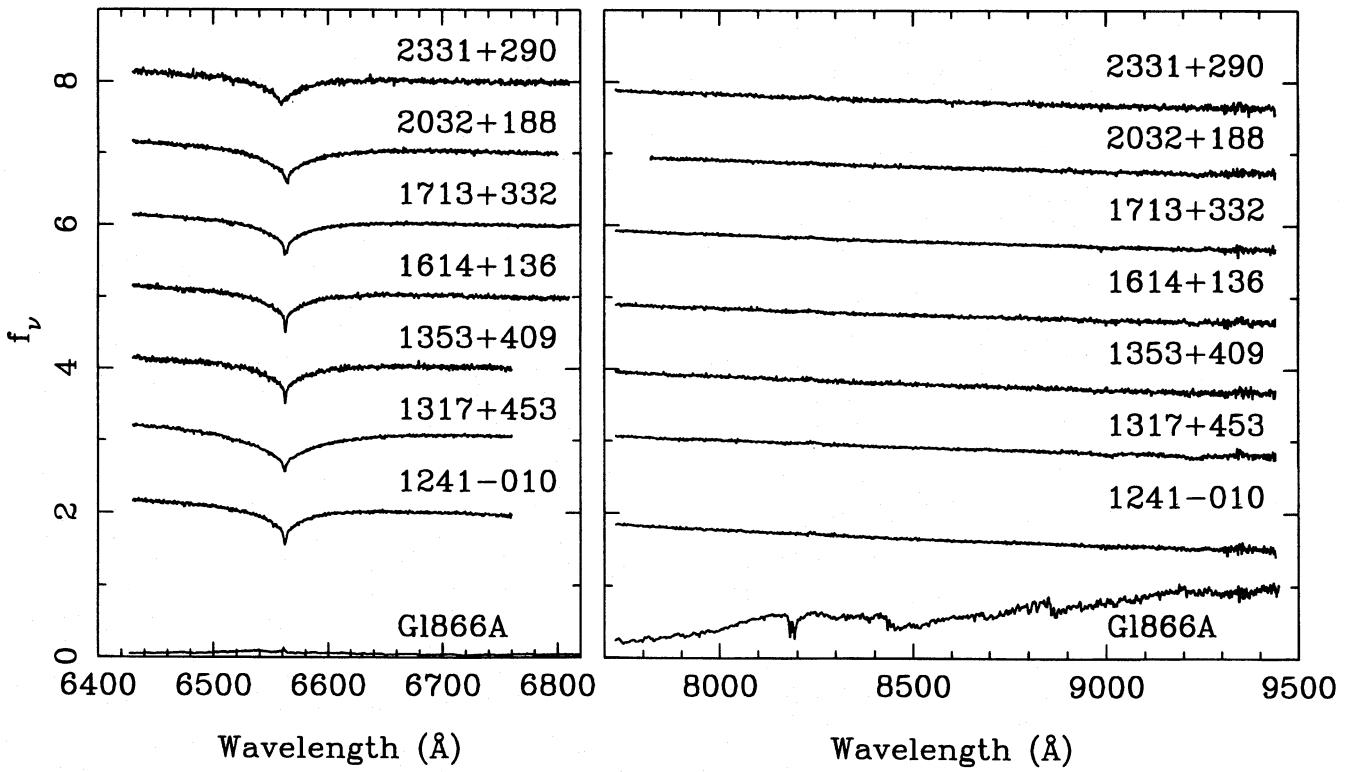

Figure 1. The mean spectra of the seven white dwarfs observed during 1993 with the 4.2-m WHT and the double-beam spectrograph ISIS. The spectra have been normalized to one at 6650 Å and are displaced vertically from one another by one unit. At the bottom we show the spectrum of an M5 dwarf observed with the same set-up. The wavelength ranges vary because of changes in the instrument set-up.

version of the difference spectrum. This is sensitive to any residual sharp features left from an incorrect subtraction. The values obtained from this method, where we have smoothed over 30 pixels and avoided regions affected by telluric absorption, are listed in Table 2 along with other information. Prior to this calculation we normalized the spectra in the range 8250 to 8400 Å, so that the fractions listed show the fraction of flux in this range that comes from an M5-type spectrum. The conclusion to be drawn from this table is that we have not detected an M star contribution in any of our targets. The 4σ upper limits are in the range 2.5 to 6 per cent, and seem to match inspection by eye after the addition of multiples of the M star spectrum. We are assuming that the spectra all have a similar shape, which may not be reasonable for very low-mass stars. However, we shall see later that the companion masses cannot be in the brown dwarf or very late-type main-sequence range, and so we do not expect significant problems from this approximation.

Our targets are classified as DA3, which have $V-I \approx -0.65$ (Greenstein 1984). If both the M star and white dwarf spectra are normalized to have the same flux in the narrow band 8250–8400 Å, the M5 star appears about 0.15 mag brighter in the I band (estimated from synthetic photometry) because the central wavelength of the I band is redward of 8400 Å. Therefore the brightest absolute I magnitudes of any late-type companions are given by $M_V + 0.65 - 0.15 - 2.5\log f$, where M_V is the absolute visual magnitude of the white dwarf and f is the 4σ upper limit to the contribution as listed in Table 2. Application of this formula gives the M_I values listed in the sixth column of Table 2.

The lower limits on M_I listed in Table 2 are at the low-mass end of the main sequence. Bessell (1991) lists M_I = 12.0, 12.5, and 13.2 for M5.5, M6 and M7 stars respectively. Translating these to M_K with the $I-K$ colours listed by Bessell (1991) and then to mass from the mass–luminosity relation of Henry & McCarthy (1993), the same values of M_I correspond to masses of 0.11, 0.10 and 0.09 $M_\odot$. Therefore our red spectra indicate that, if there are any main-sequence companions, their masses must be less than 0.1 $M_\odot$.

Fig. 2 shows an expanded view of the central core of Hα on the different nights of our run. No analysis is needed to see that there are radial velocity variations in four of the seven targets. Later on we will look at these data in more detail and show that a fifth target, 2331+290, is also a binary star. Before doing so, we consider our INT spectra of the three brightest binary candidates, 1241−010, 1317+453 and 1713+332.

3.2 The INT targets: 1241−010, 1317+453 and 1713+332

In Fig. 3 we show trailed spectra of the core of Hα for our three INT targets. We have inserted a blank spectrum between every pair of nights, but it should be realized in addition that the spectra were not taken uniformly on any given night, but were interlaced to extend the baseline on each target as far as possible. This procedure was followed in order to distinguish between aliased periods for periods below 2 d. The trailed spectra confirm the WHT detection of radial velocity variations and the variation is evidently roughly sinusoidal in 1241−010 and 1317+453. The third target 1713+332 appears

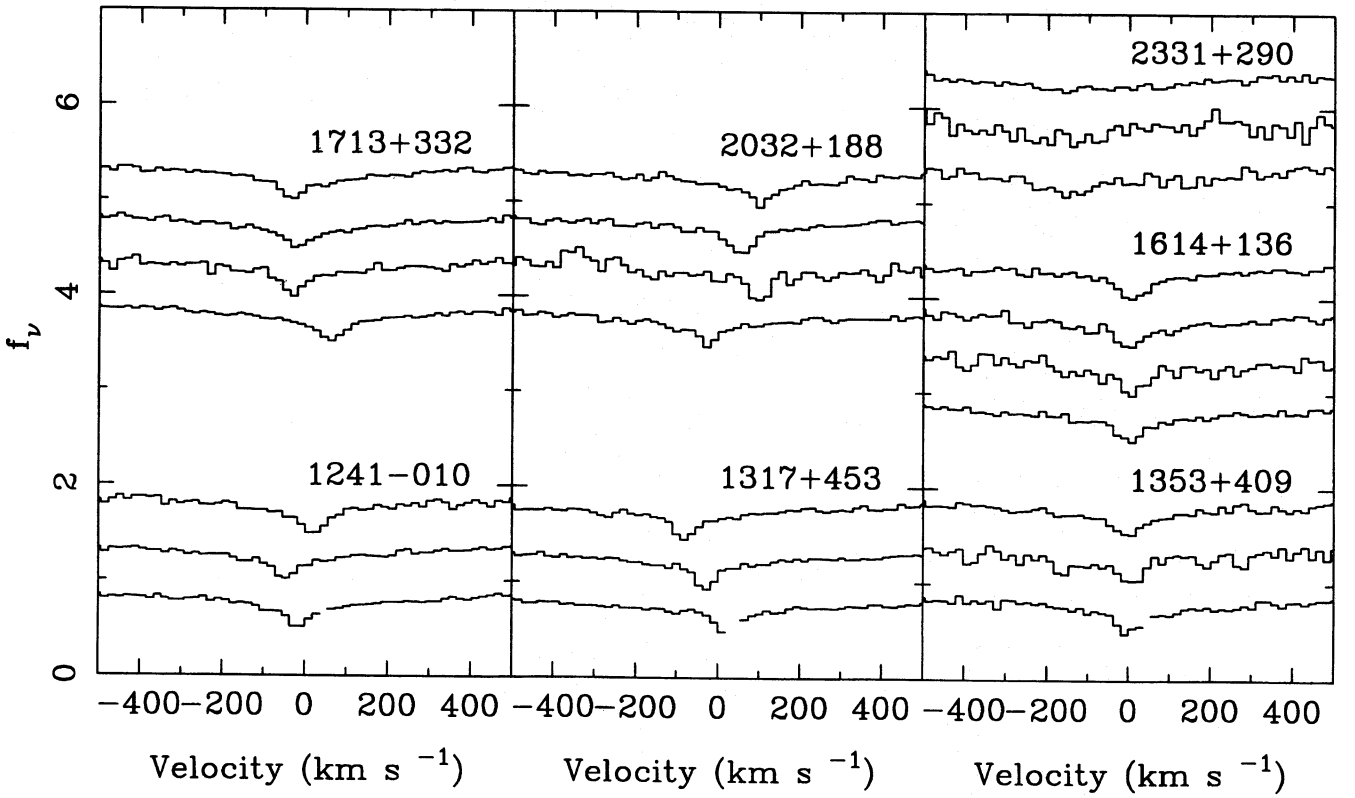

Figure 2. The figure shows the region of the spectra within $\pm 500\,\mathrm{km\,s^{-1}}$ of Hα (6562.76 Å). The spectra are the average of the data from each night separately and are plotted ascending with time. The spectra plotted in the two leftmost panels show radial velocity variability. A bad pixel has been masked in three of the spectra taken on the first night; succeeding spectra are unaffected by this pixel since we moved the grating to avoid it.

Table 2. Information on targets.

WD number[a]	V mag[b]	M_1 $M_\odot$	M_V	Fraction from [c] M5 star	M_I (4σ lower limit)
1241−010	14.02	0.31	9.32	$+0.006 \pm 0.008$	> 13.3
1317+453	14.13	0.33	10.69	$+0.007 \pm 0.006$	> 14.9
1353+409	15.43	0.40	9.88	-0.018 ± 0.013	> 14.0
1614+136	15.19	0.33	9.65	$+0.004 \pm 0.010$	> 13.4
1713+332	14.46	0.35	9.79	-0.002 ± 0.006	> 14.3
2032+188	15.34	0.36	10.24	$+0.009 \pm 0.009$	> 14.0
2331+290	15.80	0.39	9.47	$+0.019 \pm 0.014$	> 12.7

[a] The targets are referred to by the numbers listed by McCook & Sion (1987).
[b] Visual and absolute visual magnitudes and spectroscopic masses come from Bergeron et al. (1992).
[c] Normalized to 8250–8400 Å.

different, but we will see that this is a consequence of its orbital period being close to 1 d.

We measured the radial velocities of the INT and WHT spectra in the following manner (the procedure described applies to the spectra from each target and telescope independently). The spectra were first normalized by dividing by a straight line fitted between regions at $\pm$ 3600 to 4600 $\mathrm{km\,s^{-1}}$ from the centre of Hα. These regions are still affected by the broad wings, but were forced by the small chip we had to use on the INT. For consistency the same regions were used on the WHT spectra even though the latter cover a much larger range. The spectra were then averaged and fitted with a smooth model consisting of a straight line plus several Gaussian profiles. The Gaussians were fixed to have the same velocity relative to Hα (which was itself a fit parameter) but were free to vary in strength and width independently of each other. We did not use the 'pseudo-Lorentzian' model favoured by Saffer, Liebert & Olszewski (1988) and Foss et al. (1991) which can be described by

$$y = A\left(1 + \left(\frac{\lambda - \lambda_0}{\Delta\lambda}\right)^{\beta}\right)^{-1},$$

where A, $\Delta\lambda$, λ_0 and β are to be fitted. We did not use this

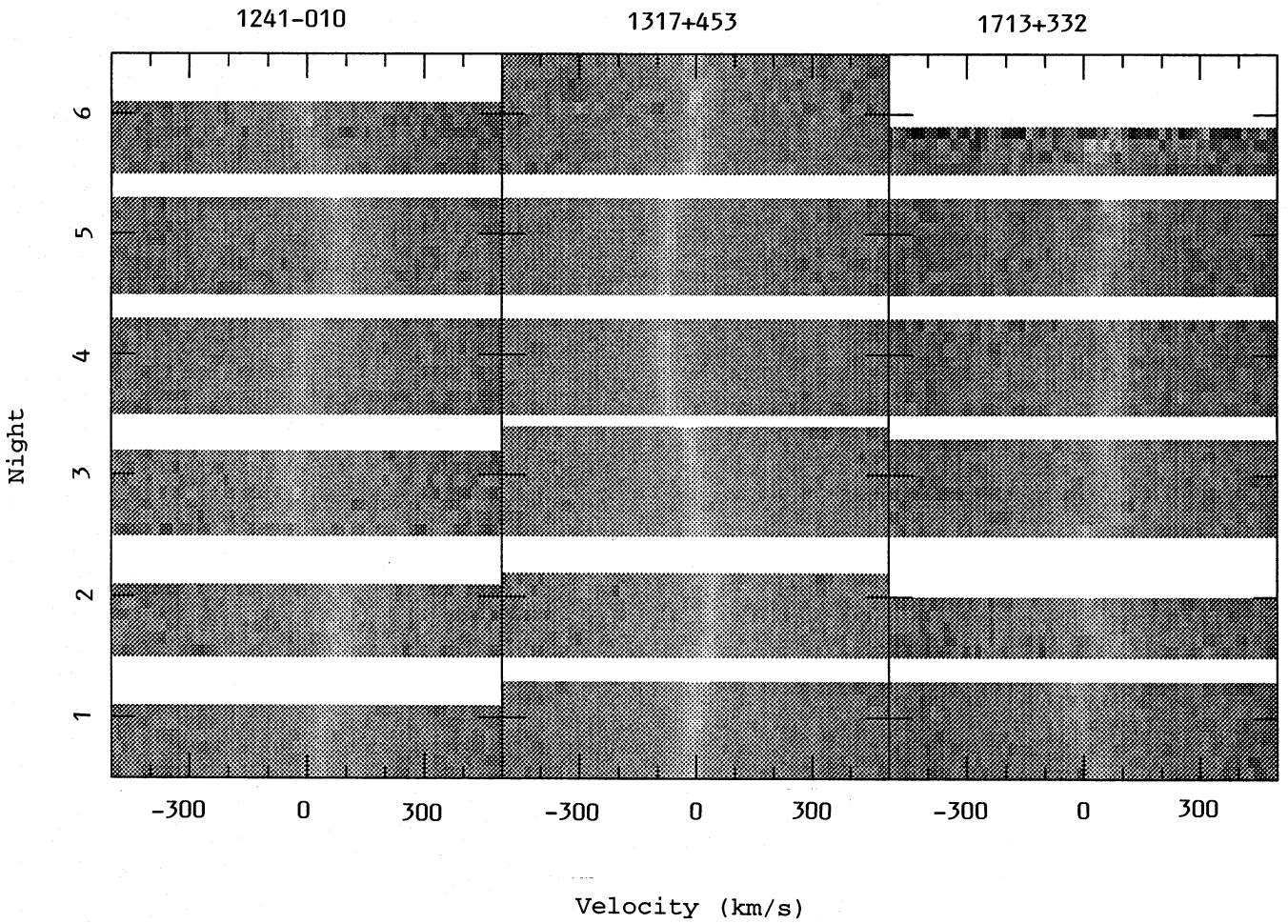

Figure 3. Trailed spectra of the three INT targets confirm the discovery of radial velocity variability and confirm the binary nature of at least two of them.

method because for our spectra additional components are required to obtain an acceptable fit (possibly because our stars are much hotter than L870 − 2, the star studied by Saffer et al.), but also because we found a tendency for the fit to lock to a position half-way between pixels. This occurred when $\beta < 1$, because then the centre of the model becomes a cusp with infinite vertical gradients with respect to the wavelength λ. This is physically impossible because of finite spectrograph resolution. Our Gaussian model avoids this problem, although it does require more parameters which can be strongly correlated with each other. These are not problems in our case as we are interested in radial velocities rather than the particular values of the other fitted parameters, and the radial velocity is not strongly correlated with any of the other fit parameters.

Armed with the fit to the average profile, all parameters were fixed apart from the straight line component and the velocity of the profile (the same value for each Gaussian component). The latter were then fitted to each spectrum separately, at the same time deriving uncertainty estimates from propagation of the uncertainties on the data through to the covariance matrix of the fit. At this point we were able to obtain our first orbital solution by fitting the velocities with a sinusoid plus a constant. Using this fit, the spectra were averaged once again with the fitted velocities removed. This sharpened the cores of the profiles considerably, and more Gaussians were needed to obtain a close fit (five in all). In Fig. 4 we show the fits to the average profiles of the INT data, and Table 3 shows the fit parameters which may be of use in simulating such profiles; the fits all reached χ^2 per degree of freedom close to unity.

Table 3. Profile fit parameters.

	1241−010	1317+453	1713+332
Constant	1.056	1.116	1.054
FWHM 1 (Å)	155.	171.	135.
FWHM 2 (Å)	78.2	82.5	68.6
FWHM 3 (Å)	27.6	27.6	26.5
FWHM 4 (Å)	7.32	7.23	7.07
FWHM 5 (Å)	1.48	1.29	1.43
Peak 1	-0.064	-0.129	-0.087
Peak 2	-0.129	-0.198	-0.127
Peak 3	-0.132	-0.116	-0.120
Peak 4	-0.082	-0.071	-0.091
Peak 5	-0.172	-0.197	-0.169

The cycle of radial velocity measurements, orbit fits, and averaging followed by Gaussian fits was repeated three times, by which time it had converged on stable values. The main

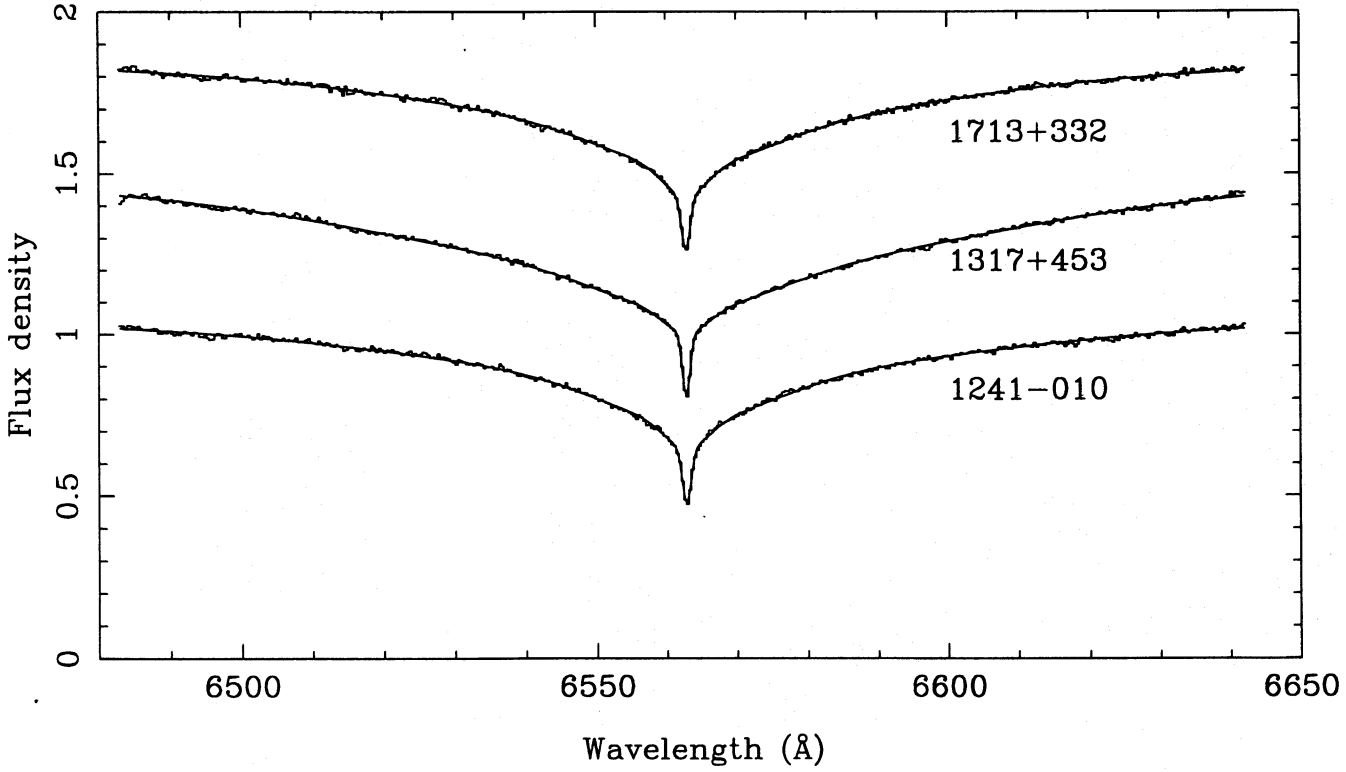

Figure 4. The mean spectra of our INT targets, corrected for orbital motion, are displayed along with the fits listed in Table 3. The spectra have been displaced by 0.4 units from each other.

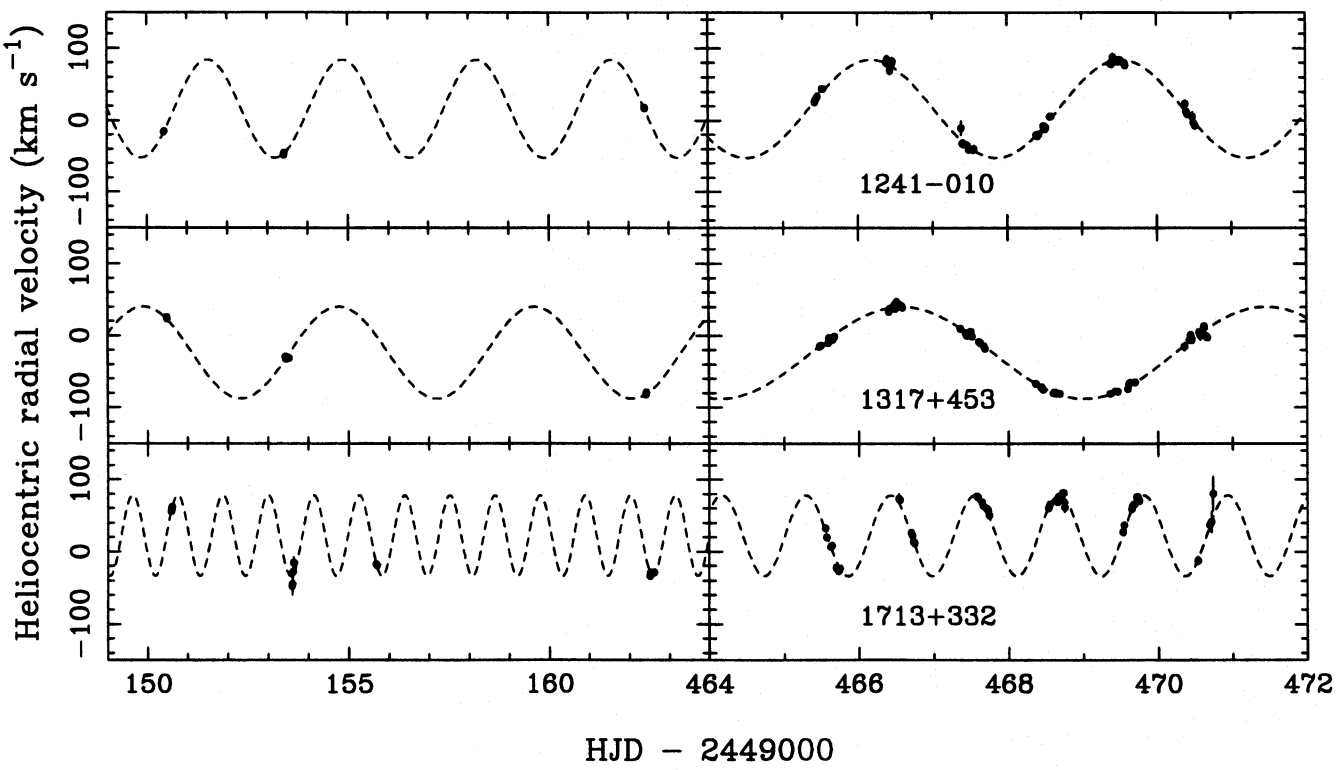

Figure 5. The radial velocities are displayed along with 1σ error bars and dashed lines showing best-fitting circular orbits. The left panels show the WHT data and the right panels show the INT data.

Table 4. Circular orbit fits.

	χ^2	N	γ km s^{-1}	K km s^{-1}	P d	$T_0 - 2449400$ d
1241−010	43.3	47	$+15.9 \pm 0.6$	68.4 ± 0.9	3.34741(14)	65.343(6)
1317+453	68.4	57	-23.8 ± 0.4	64.0 ± 0.6	4.87214(22)	65.363(6)
	72.0	57	-24.4 ± 0.4	64.5 ± 0.6	4.79783(21)	65.402(6)
1713+332	66.0	53	$+22.3 \pm 0.6$	55.8 ± 0.8	1.12740(3)	65.010(3)
	67.0	53	$+22.0 \pm 0.6$	55.8 ± 0.8	1.12338(3)	65.018(3)
2331+290	46.8	38	-11.1 ± 3.1	156.2 ± 2.9	0.1664914(7)	162.6238(8)
	53.7	38	-22.1 ± 4.3	166.0 ± 3.3	0.1997502(12)	162.6099(11)
	86.9	38	-02.6 ± 2.6	152.1 ± 2.8	0.1427274(4)	162.6331(7)

change during the process was to the uncertainties which improved considerably as the sharp core took effect.

We fitted circular orbits to all three targets. Fits to the heliocentric velocities are shown in Fig. 5, and the fit parameters and their 1σ uncertainties are tabulated in Table 4. The large gap between the WHT and INT runs means that there are closely spaced aliases for each period, and therefore we list all fits that give a χ^2 within 10 of the best value. While there is only one for 1241−010, there are two such periods for 1317+453 and 1713+332.

3.3 2331+290

We devote a separate section to this object because, although we have no spectra from the INT, we are able to tie its period down from WHT spectra taken at several epochs. Our 1993 set of WHT data showed a variation of 200 km s^{-1} in about one hour during the last night, indicating a relatively short orbital period. We therefore applied for service observations (limited to three hours maximum) in an attempt to tie down the period. On this occasion we asked for a standard set-up with Hα on the red arm of ISIS, and Hβ and Hγ on the blue arm. Scattered light rendered Hγ unusable, and so we derived velocities for Hα and Hβ only, which were added to the data from the first WHT run. There were no systematic differences between the velocities of Hα and Hβ.

The star turns out to complete almost an exact number of orbits per day, with frequencies close to 6 cycle d^{-1} the most favoured. However, there are aliases spaced by 1 cycle d^{-1} which occur in complex clusters with many peaks of similar significance. With standard methods it is hard to assess which cluster (as opposed to which single peak) is most favoured, yet this is the question of interest: before we derive a precise value of the period, we need to get somewhere near it. We adopt a Bayesian approach which allows us, amongst other things, to average the probability distribution over coarse bins (see the appendix). This allows us to decide which alias cluster is more likely. Fig. 6 shows the distribution for 2331+290 binned on coarse and fine scales. The coarse binning smoothes over the complicated alias structure and gives an idea of the relative probability of different clusters. The 6 cycle d^{-1} cluster dominates, but the 5 cycle d^{-1} cluster can also just be seen. In the absence of further information, we will assume that the 6 cycle d^{-1} cluster is the true one, although Fig. 6 is sensitive to the uncertainty estimates on the velocities, and it would not surprise us if one of the neighbouring clusters later proved to be the correct one.

The distribution of measurements, with some taken on consecutive nights and then a gap of over a year, means that

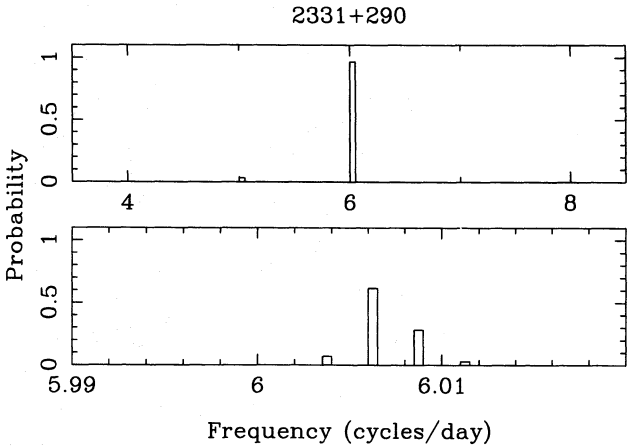

Figure 6. The figure shows the binned probability distribution for the orbital period of 2331+290 at two resolutions. The upper panel shows that the 6 cycle d^{-1} alias peak is favoured, while the lower panel shows that several peaks compete evenly inside the 6 cycle d^{-1} cluster.

each of the clusters spaced by 1 cycle d^{-1} is split into a set of aliases spaced by 0.002 49 cycle d^{-1} (or 1 cycle every 400 d). The lower panel of Fig. 6 shows a more finely binned probability distribution near 6 cycle d^{-1}. The most probable frequency is 6.006 32 cycle d^{-1}, and the best-fitting radial velocity curve is listed in Table 4 along with the best fit for the 5 and 7 cycle d^{-1} alias clusters. There are two or three close companions to each of these peaks which we have not listed to reduce confusion. We have adjusted the constant term in the ephemeris to be close to the main observing period for this object which was at the end of 1994 July. The distribution of times makes it difficult to display the data directly as in Fig. 5, and therefore in Fig. 7 we show the fit to the phase-folded data for the best orbit listed in Table 4.

Despite the statistical evidence in favour of the 6 cycle d^{-1} peak, on plotting fits to the phase-folded data there is not much to choose between the 4, 5, 6 and 7 cycle d^{-1} peaks; nevertheless, 2331+290 is clearly a short-period binary system.

3.4 The rest: 1353+409, 1614+136 and 2032+188

Of the remaining three targets, only 2032+188 shows clear radial velocity variations (Fig. 8). While it is undoubtedly a binary, we do not have enough data to establish its orbital period accurately (it was not conveniently observable during the INT run). However, a periodogram analysis suggests that the period lies in the range 2 to 10 d. The magnitude of

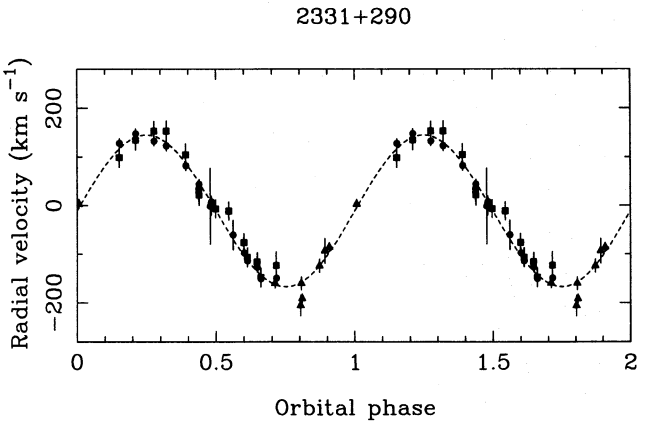

Figure 7. The phase-folded radial velocity curve of 2331+290 for $P = 0.1664913$ d. The triangles represent Hα velocities from 1993 June. Squares and circles represent Hα and Hβ measurements from 1994 July.

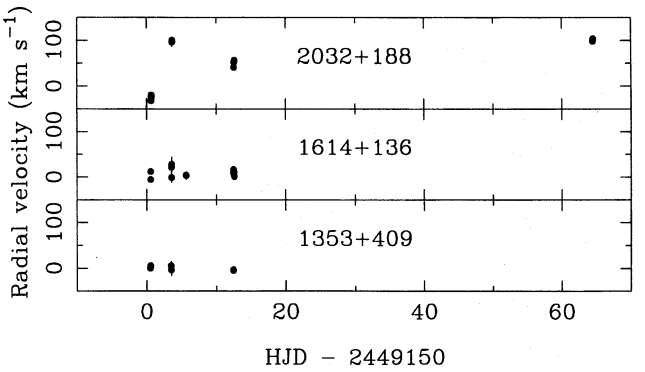

Figure 8. The radial velocities of 1353+409, 1614+136 and 2032+188.

the radial velocity variations means that the radial velocity semi-amplitude must be at least 60 km s^{-1}.

We are left with two stars, 1353+409 and 1614+136, which show no sign of a binary companion at all. There is of course some chance that they are binaries, but were not detected as such, perhaps because of bad luck with the times or because we see their orbits almost face-on. We will consider this quantitatively in the discussion section.

4 DISCUSSION

4.1 The masses and nature of the companions

Measurement of the orbital period P and semi-amplitude K of a binary star gives the so-called mass function $f(M_1, M_2)$ given by

$$f(M_1, M_2) = \frac{M_2^3 \sin^3 i}{(M_1 + M_2)^2} = \frac{PK^3}{2\pi G},$$

where i is the orbital inclination and M_1 and M_2 are the component stars' masses. We adopt the convention that M_1 is the mass of the brighter star and M_2 the mass of its unseen companion. The mass function puts a lower limit upon the mass of the companion M_2 which is reached only if the system is edge-on with $i = 90°$ and $M_1 = 0$. Under just these

Table 5. Mass functions.

Target	$f(M)$ $M_\odot$	M_2 $M_\odot$, lower limit.
1241−010	0.111 ± 0.005	0.373 ± 0.022
1317+453	0.132 ± 0.004	0.421 ± 0.024
1713+332	0.020 ± 0.001	0.178 ± 0.006
2331+290	0.066 ± 0.004	0.322 ± 0.014

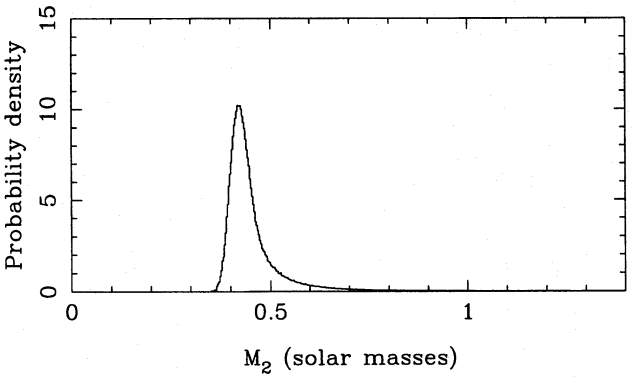

Figure 9. The probability distribution for the companion mass assuming that it is the same for the four binaries with measured periods.

weak conditions, the mass functions of our targets, which are listed in Table 5 (for our best-fitting periods in each case), indicate masses greater than 0.1 $M_\odot$ for two of our targets, corresponding to late M dwarfs if they are main-sequence stars. In this case, we know the masses M_1 of the brighter components since they were fitted by Bergeron et al. (1992). Assuming these values, with uncertainties of 0.03 $M_\odot$, we get the much larger lower limits on M_2 listed in Table 5. These again are only reached if $i = 90°$.

The revised lower limits remove the possibility that the companions can be main-sequence dwarfs since, as we saw in Section 3.1, any M dwarf companion must have a mass below 0.1 $M_\odot$ to remain undetectable. For example, we estimate that a 0.18-$M_\odot$ M dwarf has $M_I \approx 10.3$, some four magnitudes brighter than the limit set upon 1713+332, the star with the smallest possible companion. The only alternative is that the companions are also compact stars, with white dwarfs by far the most likely possibility. With only four measurements, it is too early to say much in detail about the companion masses. However, as a start, if we assume that all the companions have the same mass, and that our systems have been selected from randomly inclined orbits, we can make a statistical estimate of the unique mass. Fig. 9 shows the distribution obtained by Monte Carlo integration. There is a 99.6 per cent chance that the mass is below 1 $M_\odot$ and a 92 per cent chance that it is below 0.55 $M_\odot$, the mean mass for isolated white dwarfs from Bergeron et al. (1992). Since all well-determined masses for neutron stars are close to 1.4 $M_\odot$, the companions are most likely to be white dwarfs, with marginal evidence that they may be less massive than isolated white dwarfs. The latter result needs to be confirmed with more data, but would not be surprising since binary interaction could affect the evolution of both stars.

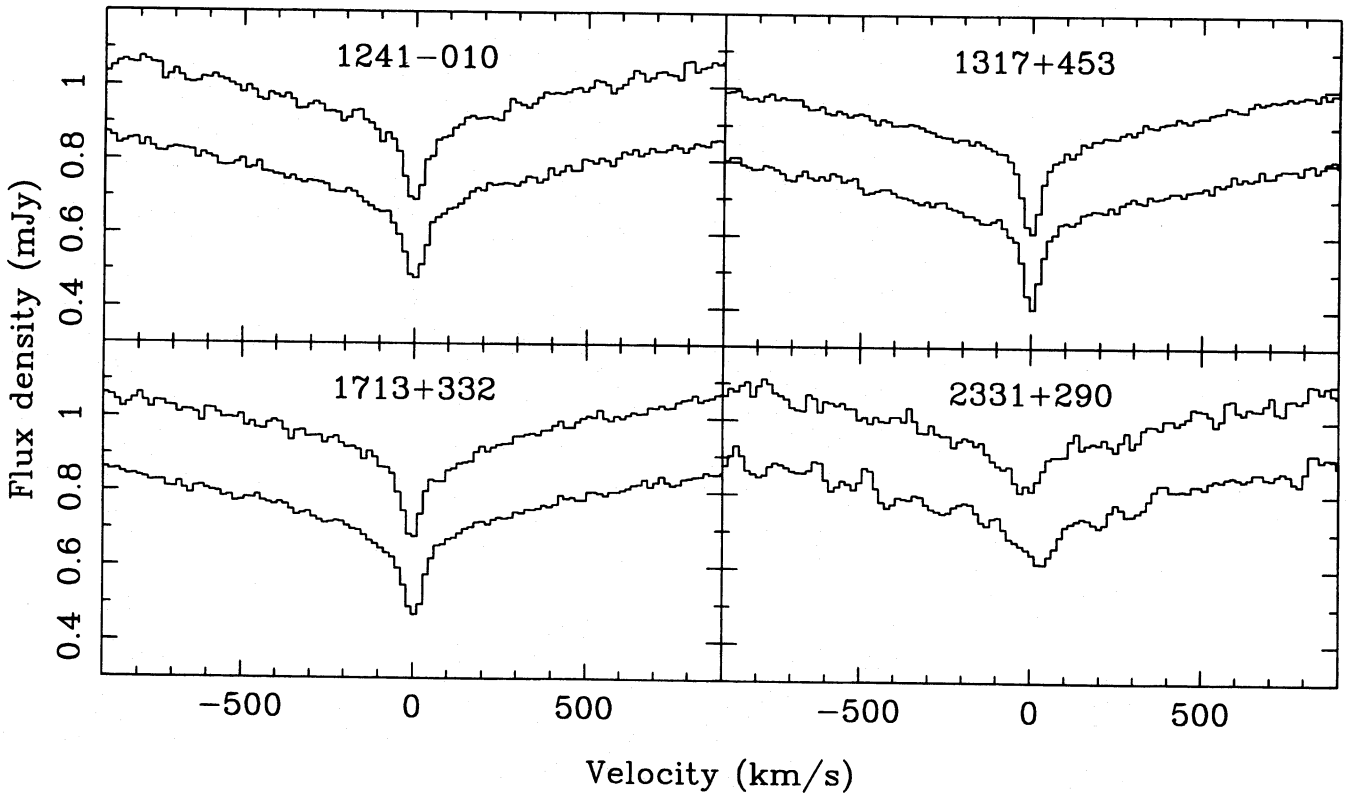

Figure 10. The spectra averaged around the quadrature phases for four of the binaries. The lower spectrum of each pair is the average over the orbital phase range 0.1 to 0.4 during which the companion moves towards us (blueshifted), whereas the upper spectrum is the average over the range 0.6 to 0.9. 1713+332 shows an asymmetry (most obvious within $\pm 200\,\mathrm{km\,s^{-1}}$ of the line centre) of the nature expected for a significant contribution from the companion star.

4.2 Limits upon the brightness of the companions

As the companion stars are also white dwarfs, they may have spectra similar to the primary star and therefore may be difficult to detect even if they are of similar brightness. Worse, there is no reason to expect them to be of similar brightness as the companion may be much cooler than the star we can see. We searched for signs of the companion stars by shifting out the fitted radial velocity for each binary, and then averaging the spectra over two intervals, 0.1 to 0.4 and 0.6 to 0.9, which cover the quadrature phases 0.25 and 0.75.

If there is a contribution from a companion white dwarf, it should be visible as an asymmetry in the line profile which should swap sign between the two quadrature phases. Furthermore, at phase 0.25, the profile should appear depressed on the blueshifted side of the core, and vice versa at phase 0.75. In Fig. 10 we plot these spectra for each of our targets. There is no obvious asymmetry in 1241−010, 1317+453 or 2331+290. 1713+332, however, does show the expected asymmetry, from which we deduce that the companion spectrum is just detectable. Thus 1713+332 joins L870−2 ($P = 1.5578$ d; Saffer et al. 1988) as a double-lined, close double-degenerate binary star.

Our data are not of high enough resolution to decompose the two spectra in 1713+332. We have carried out simulations which indicate that, if the companion's spectrum is similar to that of the primary star, then it must contribute about 10 to 20 per cent of the light. At the same time, these simulations show that, as might be expected, the presence of the companion's spectrum reduces the radial velocity semi-amplitude which is therefore probably greater than the $56\,\mathrm{km\,s^{-1}}$ we measured for 1713+332 by 1 or $2\,\mathrm{km\,s^{-1}}$. Clearly, higher resolution data are needed to obtain the radial velocities of each component separately.

4.3 2331+290: a future merger

At 4 h, 2331+290 has the shortest period of any of our targets. At such a short period, angular momentum loss through gravitational radiation becomes effective, and eventually will cause the binary to merge. Gravitational radiation causes a loss of angular momentum at a rate given by

$$\frac{\dot{J}}{J} = -\frac{32}{5}\frac{G^3}{c^5}\frac{M_1 M_2 (M_1 + M_2)}{a^4},$$

where a is the separation (Landau & Lifshitz 1958). Integrating and substituting for a in terms of the orbital period, we find that the time to merger is given by

$$\tau_\mathrm{m} = 1.00 \times 10^7 \frac{(M_1 + M_2)^{1/3}}{M_1 M_2} P^{8/3}\ \mathrm{yr}$$

where the orbital period P is in units of hours and the masses are measured in solar units. Taking $M_1 = 0.39\,\mathrm{M_\odot}$ and $P = 4\,\mathrm{h}$ from Tables 2 and 4, and assuming that $M_2 = 0.5\,\mathrm{M_\odot}$, we find $\tau_\mathrm{m} = 2 \times 10^9$ yr (if the 5 cycle $\mathrm{d^{-1}}$ alias is correct then this must be increased by a factor of 2). This is less than the age of the Galaxy and therefore 2331+290 is representative of a population of merging white dwarfs. Mergers of white dwarfs

with a combined mass greater than the Chandrasekhar limit of 1.4 $M_\odot$ may result in type Ia supernovae. It is very unlikely, however, that 2331+290 is this massive.

4.4 Common-envelope fossils

Although we have shown that gravitational radiation will cause 2331+290 to merge on a relatively short time-scale, we can also show that it is still sufficiently weak that there has been very little change in its orbital period, or the orbital periods of any of the other targets since they emerged from the common envelope. The temperatures of our targets were determined from model atmospheres by Bergeron et al. (1992), and these can be used to limit the time since the common-envelope phase. 2331+290 has a temperature of 27 000 K, which indicates an age since the common-envelope phase of order 10^7 yr (Mazzitelli & D'Antona 1986). This is much shorter than the gravitational radiation time-scale, which is shortest for 2331+290.

Therefore the orbital periods that we observe are essentially the same as they were immediately after the ejection of the envelope. This makes binary white dwarfs particularly useful as constraints upon common-envelope evolution. With enough systems it will become possible to make precise comparisons between theory and observation. We are not at this stage yet, with only six systems of known orbital period. However, a crude comparison shows that the theoretical prediction cannot be too far out. Yungelson et al. (1994) present a theoretical prediction of the orbital period distribution which is fairly flat from 2 h to 1.3 d, falling steeply outside these limits, although there is a significant tail to longer periods which finally cuts off at about 10 d. The known systems have periods of 1.56 d (Saffer et al. 1988), 1.18 d (Bragaglia et al. 1990), and 0.167, 1.13, 3.35 and 4.87 d (this paper). (Reid, Saffer & Liebert (1993) have also found an sdB star in an orbit of period 0.206 d, but the nature of its companion is not determined.) The observed and predicted distributions seem to be in reasonable agreement, with a suggestion that the observed periods are a bit longer than expected.

The theoretical prediction was made (Yungelson et al. 1994) with an envelope ejection efficiency, $\alpha_{CE} = 1$, about the maximum expected, without the addition of non-orbital sources of energy. If α_{CE} is much less, then the binaries lose more energy in ejecting the envelope and end up at shorter periods. An idea of the change possible is given in Yungelson, Tutukov & Livio (1993) where a change in α_{CE} from 1.0 to 0.1 shifts the peak in the period distribution from around a day to less than 0.01 d. Therefore the six known double-degenerate systems suggest that α_{CE} as used by Yungelson et al. (1994) is close to 1 and that the common-envelope ejection is efficient.

4.5 Can 1353+409 and 1614+136 be binaries?

Given that five out of seven targets are binaries, we have to consider whether the remaining targets, 1353+409 and 1614+136, could also be binaries that we have missed because of ill-luck. In the appendix we extend our Bayesian analysis to obtain, given a set of radial velocity measurements, the probability that a star is a binary as opposed to a single star. As we explain in the appendix, this is different from the usual technique which is to derive the probability that the data could have been obtained from noise alone (Scargle 1982; Horne & Baliunas 1986). In our opinion these two probabilities are not equivalent, and, as we show in the appendix, the Bayesian answer is normally considerably more conservative in the sense that it is less likely to indicate that a detection has been made. Bayesian computations require the specification of prior probabilities. We made the following assumptions.

Table 6. Binary to single star log probability ratios.

WD number	$\log \frac{P(\text{binary})}{P(\text{single})}$		
	A [a]	B	C
1241−010	91.1	92.8	93.4
1317+453	563.7	565.7	566.4
1353+409	−5.6	−4.6	−4.5
1614+136	−5.9	−5.5	−5.0
1713+332	361.7	362.8	362.8
2032+188	285.9	287.3	287.4
2331+290	50.7	50.2	53.3

[a] Column A values are for a prior probability uniform over frequency f. Column B is for uniformity in $\ln f$, and column C is for a prior uniform in orbital period P.

(i) We integrated over periods from 1 h to 50 d, with three different weightings. These were uniform in frequency f, uniform in $\ln f$ or equivalently $\ln P$ where P is the orbital period, and uniform in orbital period P.

(ii) We used a prior range of systemic velocities of $\pm 250\,\mathrm{km\,s^{-1}}$ equivalent to $R_\gamma = 500\,\mathrm{km\,s^{-1}}$ (see appendix).

(iii) The prior range of K_X and K_Y was $\pm 1000\,\mathrm{km\,s^{-1}}$ for a period $P = 1$ d. This range R was scaled with P to keep R^3P, which is proportional to the mass of the system, constant.

(iv) We assumed a prior probability ratio of binary star versus single star of 1 in 100, in rough accord with the paucity of white dwarf binary stars in previous surveys.

All of these assumptions are uncertain. For instance, the period distribution predicted by Yungelson et al. (1994) is concentrated between 2 h and 1.3 d rather than 1 h to 50 d, but what matters in the end is whether the uncertainty is overwhelmed by the data. The probability ratios calculated for the three weightings over period are listed in Table 6. We have only included the 1993 WHT data in these calculations (obviously the additional data from the INT improve the detections still more). In five cases the probability indicates that the star is a binary star, and even in the most marginal case, 2331+290, the ratio is large enough to exceed any reasonable uncertainty in the prior probabilities.

By contrast, the log probability ratios for the two non-detections are not so far below zero as to remove all possibility of their being binaries. Our assumptions above were slanted against the binary hypothesis, since initially we need to be convinced that our targets are binaries. Having done so, and given the absence of credible alternatives to the binary model for low-mass white dwarfs, we really need to be convinced that 1353+409 and 1614+136 are *not* binaries. Thus we should change the above assumptions to be closer to what we know of such binaries. First the range of K_X above allows companions up to 100 $M_\odot$. Such a wide range is conservative when trying to detect binary motion, but on the binary model it is almost certain that the companion has a mass below 1.4 $M_\odot$. Thus the prior range can be lowered to $200\,\mathrm{km\,s^{-1}}$ (defined for

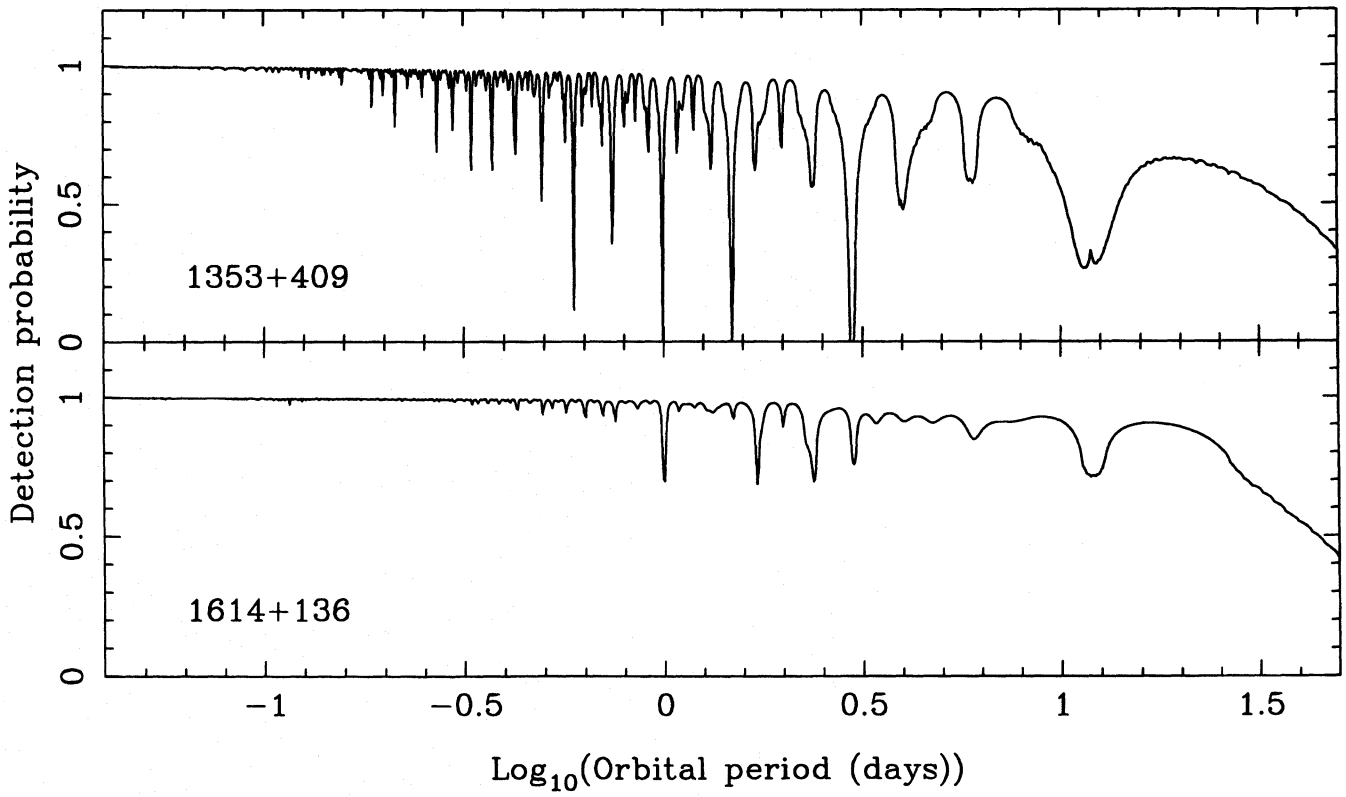

Figure 11. The detection probability as a function of orbital period based on the calculation described in the text. A change in assumed prior probabilities by a factor of 100 changes the detection probability by at most 10 per cent at long periods, and less at short periods.

an orbital period of 1 d). This reduces the prior space for the binary model by $(1000/200)^2 = 25$. The prior probability should now reflect our bias that all low-mass white dwarfs are binary stars, allowing for the possibility of experimental error and for some unknown route via single star evolution. Thus a change from 100:1 in favour of single stars to perhaps 10:1 in favour of binary stars would not be unreasonable.

With these changes, the posterior probability for 1353+409 and 1614+136 being binary stars rises to $\approx$ 10 per cent. Given other uncertainties, such as the possibility of very low-mass main-sequence star companions, we conclude that there is room for these two stars to be binaries in about the right period range. This is almost a trivial conclusion. Of course there is always going to be some chance that a star is a binary but not detectable as such. The point here is that the chance is a significant one. This conclusion was not inevitable; with a much larger dataset it will become possible to make a firm decision for or against these stars being binaries.

Another way of looking at this question is to compute the probability, given that 1353+409 and 1614+136 *are* binaries, that we detect them as such. To estimate this, we calculated the radial velocity amplitude needed to produce a 1:1 probability ratio estimated in the same way as for Table 6, except now it is not integrated over period. We used the same times and radial velocity uncertainties as obtained on the target of interest. Assuming randomly inclined orbits with random phases and a companion mass of $0.5\,M_\odot$, we can then calculate the fraction of binaries that would have been detected, as a function of orbital period. We call this the detection probability. The results are plotted in Fig. 11.

The calculations leading to Table 6 are very time-consuming, and therefore for Fig. 11 we did not carry out the full integration over period for each assumed period, but just used the value of the integrand at the assumed period, which should be close to the peak value. In general we have found that the full integral is 1–2 less in the log than the peak value of the integrand. Therefore we set detection thresholds two units above the true level, using values of log binary/single = 2.

Fig. 11 shows that our detection probability was higher than 90 per cent for most periods below about 5 d. However, there is a reasonable chance, especially at long periods, that we would not have detected binary motion, and this is consistent with the calculations outlined above. As we mentioned before, Yungelson et al. (1994) predict that most systems should be found with P between 2 h and 1.3 d which is a region of high detection probability. However, we have already found two systems with periods longer than this, and so we believe that it is still possible that 1353+409 and 1614+136 are also binaries. Further observations of these systems would be of interest.

5 CONCLUSIONS

We have detected five close binaries out of seven white dwarfs selected for their low mass, confirming the idea that binary interaction is needed to produce low-mass white dwarfs. We have measured the orbital parameters of four of these, which, together with the lack of any late-type stellar features, show that their companions are also white dwarfs.

One of our discoveries (2331+290) is a binary white dwarf of short enough period to merge within a Hubble time. However, all of the targets are young enough that their periods have changed little since they emerged from a common envelope. The orbital periods that we have observed, in particular 1241−010 and 1317+453 with periods of 3.35 and 4.87 d, suggest that the common envelope is ejected efficiently with $\alpha_{CE} \approx 1$.

Another of our discoveries, 1713+332, is a double-lined binary, although we could not resolve the two component spectra cleanly.

ACKNOWLEDGMENTS

TRM was supported by a PPARC Advanced Fellowship during the course of most of this work. SRD was supported on a PPARC post-doctoral grant. We thank the La Palma staff for obtaining the service data so speedily.

REFERENCES

Bergeron P., Saffer R.A., Liebert J., 1992, ApJ, 394, 228
Bessell M.S., 1991, AJ, 101, 662
Bragaglia A., Greggio L., Renzini A., D'Odorico S., 1990, ApJ, 365, L13
Foss D., Wade R.A., Green R.F., 1991, ApJ, 374, 281
Greenstein J.L., 1984, ApJ, 276, 602
Gregory P.C., Loredo T.J., 1992, ApJ, 398, 146
Henry T.J., McCarthy D.W.J., 1993, AJ, 106, 773
Horne J.H., Baliunas S.L., 1986, ApJ, 302, 757
Iben I., Livio M., 1993, PASP, 105, 1373
Kirkpatrick J.D., Henry T.J., McCarthy D.W.J., 1991, ApJS, 77, 417
Landau L., Lifshitz E., 1958, The Theory of Classical Fields. Pergamon Press, Oxford
McCook G.P., Sion E.M., 1987, ApJS, 65, 603
Mazzitelli I., D'Antona F., 1986, ApJ, 311, 762
Reid N., Saffer R.A., Liebert J., 1993, in Barstow M., ed., White Dwarfs: Advances in Observation and Theory. Kluwer Academic Publishers, Dordrecht, p.441
Robinson E.L., Shafter A.W., 1987, ApJ, 322, 296
Saffer R.A., Liebert J., Olszewski E., 1988, ApJ, 334, 947
Scargle J.D., 1982, ApJ, 263, 835
Sweigart A.V., 1994, ApJ, 426, 612
Yungelson L.R., Tutukov A.V., Livio M., 1993, ApJ, 418, 794
Yungelson L.R., Livio M., Tutukov A.V., Saffer R.A., 1994, ApJ, 420, 336
Zuckerman B., Becklin E.E., 1992, ApJ, 386, 260

APPENDIX A: BAYESIAN PROBABILITY ANALYSIS

We now derive quantitative measures for the binary-star model versus the single-star model for each of our targets. We adopt a Bayesian approach to answer the question 'what is the ratio of the probability that the target is a binary star to the probability that it is a single star?'. In essence we wish to estimate the probability ratio of the hypothesis that the target is a member of a binary (denoted by B) and the hypothesis that it is a single star (S), given the data, that is, $P(B|D)/P(S|D)$. Using Bayes' theorem, the probabilities can be expressed as:

$$P(B|D) = \frac{P(D|B)P(B)}{P(D)}, \tag{A1}$$

and similarly for $P(S|D)$. The probability $P(D)$ is common to both hypotheses and cancels out. The probability $P(B)$ and its counterpart $P(S)$ are the a priori probabilities in favour of each model; we will consider them in more detail later. We now calculate the probability $P(D|B)$. We assume that we have measured velocities V_i at times t_i and that they are independent Gaussian random variables with standard deviations σ_i, where i runs from 1 to N, the number of data points. We are only interested in binaries that have interacted and therefore have circular orbits, such that the predicted velocities V_i' are given by

$$V_i' = \gamma + K_X \cos\Omega t_i + K_Y \sin\Omega t_i,$$

where γ, K_X, K_Y and Ω are parameters of the binary model. In the single-star case the predicted velocities are fitted by $V_i' = \gamma$, a single-parameter model. To obtain $P(D|B)$ we have to integrate over the parameters of the model:

$$P(D|B) = \int\int\int\int P(D|\gamma,K_X,K_Y,\Omega) \times P(\gamma,K_X,K_Y,\Omega)\,d\gamma\,dK_X\,dK_Y\,d\Omega, \tag{A2}$$

where $P(D|\gamma,K_X,K_Y,\Omega)$, sometimes called the likelihood, is given by

$$P(D|\gamma,K_X,K_Y,\Omega) = \left(\prod_j \frac{w_j}{2\pi}\right)^{1/2} \times \exp -\frac{1}{2}\sum_i w_i(V_i - V_i')^2, \tag{A3}$$

and $w_i = 1/\sigma_i^2$. We assume that the parameters are independent so that the joint probability above factorizes. The model depends linearly upon the parameters γ, K_X, and K_Y. These can adopt negative or positive values and we assume uniform prior distributions of each parameter between values of $\pm R_\gamma/2$ for the systemic velocity, and $\pm R_K/2$ for each of the amplitudes. Strictly speaking, it would probably be better to use the total amplitude $K = (K_X^2 + K_Y^2)^{1/2}$ and the orbital phase, since we could assume a uniform distribution of phase zero-points, but we shall see that it is not normally important.

The linear parameters can be integrated out analytically if the priors cover a volume of parameter space large enough for us to be able to set the integration limits to $\pm\infty$. This assumption is most likely to break down at low frequencies where it is possible to have large amplitudes but still fit the data. We did test for the breakdown of this assumption, but it had little effect upon the results presented here. On integrating (at a specific frequency Ω) we find

$$\frac{P(B,\Omega|D)}{P(S|D)} = \frac{P(B,\Omega)}{P(S)} \frac{(2\pi)^{3/2}}{R_K^2 R_\gamma (\det\mathbf{A})^{1/2}} \frac{R_\gamma (\sum_i w_i)^{1/2}}{(2\pi)^{1/2}} \times \exp\frac{1}{2}\left(\mathbf{b}^t\mathbf{A}^{-1}\mathbf{b} - \frac{(\sum_i w_i V_i)^2}{\sum_j w_j}\right), \tag{A4}$$

where the vector $\mathbf{b}$ is given by

$$\mathbf{b} = \begin{pmatrix} \sum_i w_i \\ \sum_i w_i c_i \\ \sum_i w_i s_i \end{pmatrix}$$

and the symmetric matrix **A** is given by

$$\mathbf{A} = \begin{pmatrix} \sum_i w_i & \sum_i w_i c_i & \sum_i w_i s_i \\ \sum_i w_i c_i & \sum_i w_i c_i^2 & \sum_i w_i c_i s_i \\ \sum_i w_i s_i & \sum_i w_i c_i s_i & \sum_i w_i s_i^2 \end{pmatrix}$$

where $c_i = \cos\Omega t_i$ and $s_i = \sin\Omega t_i$. The exponent in equation (A4) is closely related to the periodogram of Scargle (1982). Indeed, exactly Scargle's periodogram is obtained as the exponent if we compare the two models with γ fixed to be zero. We could have subtracted the mean of the data in order to satisfy Scargle's model, but this is not exactly equivalent to having the constant as one of the parameters, particularly for small numbers of data points as we have here. In addition to the exponential, equation (A4) has three factors peculiar to the Bayesian analysis, all of which tend to favour the constant model. The first factor is the prior probability ratio, which, if we are cautious, we should weight towards the single-star hypothesis. This factor is not usually considered, but it is obviously important. For instance, suppose we knew for certain from other evidence that our target was not a binary, then it would not matter how strongly the data showed periodic behaviour, we would have to favour the single-star model.

The second factor comes from the integration over the 'nuisance' parameters of the binary model, and is in the form of a dimensionless ratio of the volume of parameter space allowed by the data, $(\det\mathbf{A})^{-1/2}$, divided by the prior volume $(R_K^2 R_\gamma)$. Similarly, the third factor comes from the integration of the single-star model giving the volume allowed by the data $(\sum_i w_i)^{-1/2}$ relative to the prior range R_γ. Together these factors represent the penalty paid for allowing a more flexible model. Although the binary model is bound to fit the data better than the single-star model because it contains the latter as a special case, it only does so in a small fraction of parameter space. For example, suppose that $R_\gamma = R_K = 1000\,\mathrm{km\,s^{-1}}$, and that our data are good enough to measure γ, K_X and K_Y to $10\,\mathrm{km\,s^{-1}}$. Then the second factor is of order 10^{-6} whereas the third is of order 10^2, giving a total ratio in favour of the single-star model of 10^4.

Along with the prior ratio, which we may expect to favour the single-star model, the factors in front of the exponential may multiply up to of order 10^6 in favour of the single-star model, and so the exponent must exceed ≈ 15 before the binary model becomes favoured at all. This is very conservative compared to standard applications of Scargle's (1982) analysis. If we take the artificial (but comparable) case of a single known period, then Scargle shows that a peak of height z or more will be produced by random noise with probability e^{-z}. (We assume here that Scargle's function is exactly equivalent to the exponent in equation (A4), although, as we remarked above, this is only the case when the systemic velocity is not included.) The probability of observing a Gaussian random variable more than 3σ from the mean is 0.0026, and therefore we might take a peak of $z = -\ln 0.0026 \approx 6$ to indicate a '3σ' detection of a known period, and therefore of a binary nature for the star of interest. However, the quantity of interest is not the chance that random noise produces such a signal, but the probability that our target is a binary star, and the two quantities are not the same. To get the same '3σ' probability, the Bayesian calculation suggests that a peak of order 21 is needed, equivalent to a '6σ' detection on Scargle's analysis. Therefore in our opinion the normal method is inclined to produce detections too easily. Clearly the prior ranges and prior odds in favour of one model against the other are uncertain, but this just means that we should choose them pessimistically (as we have) or equivalently set a high enough detection threshold to offset any reasonable variation in the prior probabilities. As we see it, this uncertainty is incorrectly ignored in the 'frequentist' approach. A similar point has been made in the more general analysis of Gregory & Loredo (1992). As it happens, our targets are well separated into detections and non-detections (Table 6), and we would have reached the same conclusions with either method.

The above discussion was based on a search for a known period, but in reality we don't know the orbital period in advance and so we need to integrate to obtain the final probability ratio:

$$\frac{P(B|D)}{P(S|D)} = \frac{1}{P(S|D)} \int P(B,\Omega|D) P(\Omega)\,\mathrm{d}\Omega. \qquad \text{(A5)}$$

This integration must be carried out numerically. More uncertainty is introduced here as we cannot be sure of the prior distribution for the orbital period or equivalently Ω, but as remarked above this only forces us to be more careful about the detection threshold. The values of $\log P(B|D)/P(S|D)$ for our targets are listed in Table 6.

This paper has been produced using the Royal Astronomical Society/Blackwell Science LaTeX style file.